arXiv:2009.01513v2 [astro-ph.HE] 4 Sep 2020

Discovery of a Gamma-ray Black Widow Pulsar by GPU-accelerated Einstein@Home

L. NIEDER,[1,2] C. J. CLARK,[3] D. KANDEL,[4] R. W. ROMANI,[4] C. G. BASSA,[5] B. ALLEN,[1,6,2] A. ASHOK,[1,2] I. COGNARD,[7,8]
H. FEHRMANN,[1,2] P. FREIRE,[9] R. KARUPPUSAMY,[9] M. KRAMER,[9,3] D. LI,[10,11] B. MACHENSCHALK,[1,2] Z. PAN,[10] M. A. PAPA,[1,6,2]
S. M. RANSOM,[12] P. S. RAY,[13] J. ROY,[14] P. WANG,[10] J. WU,[9] C. AULBERT,[1,2] E. D. BARR,[9] B. BEHESHTIPOUR,[1,2] O. BEHNKE,[1,2]
B. BHATTACHARYYA,[14] R. P. BRETON,[3] F. CAMILO,[15] C. CHOQUET,[16] V. S. DHILLON,[17,18] E. C. FERRARA,[19,20] L. GUILLEMOT,[7,8]
J. W. T. HESSELS,[5,21] M. KERR,[13] S. A. KWANG,[6] T. R. MARSH,[22] M. B. MICKALIGER,[3] Z. PLEUNIS,[23,24] H. J. PLETSCH,[1]
M. S. E. ROBERTS,[25,26] S. SANPA-ARSA,[27] AND B. STELTNER[1,2]

[1]Max-Planck-Institut für Gravitationsphysik (Albert-Einstein-Institut), 30167 Hannover, Germany
[2]Leibniz Universität Hannover, 30167 Hannover, Germany
[3]Jodrell Bank Centre for Astrophysics, Department of Physics and Astronomy, The University of Manchester, M13 9PL, UK
[4]KIPAC/Dept. of Physics, Stanford University, Stanford, CA 94305, USA
[5]ASTRON, The Netherlands Institute for Radio Astronomy, Oude Hoogeveensedijk 4, 7991 PD Dwingeloo, The Netherlands
[6]Department of Physics, University of Wisconsin-Milwaukee, P.O. Box 413, Milwaukee, WI 53201, USA
[7]Laboratoire de Physique et Chimie de l'Environnement et de l'Espace, Université d'Orléans / CNRS, F-45071 Orléans Cedex 02, France
[8]Station de radioastronomie de Nançay, Observatoire de Paris, CNRS/INSU, F-18330 Nançay, France
[9]Max-Planck-Institut für Radioastronomie, auf dem Hügel 69, 53121 Bonn, Germany
[10]National Astronomical Observatories, Chinese Academy of Sciences, Beijing 100101, China
[11]NAOC-UKZN Computational Astrophysics Centre, University of KwaZulu-Natal, Durban 4000, South Africa
[12]National Radio Astronomy Observatory, 520 Edgemont Rd., Charlottesville, VA USA 22903
[13]Space Science Division, Naval Research Laboratory, Washington, DC 20375-5352, USA
[14]National Centre for Radio Astrophysics, Tata Institute of Fundamental Research, Pune 411 007, India
[15]South African Radio Astronomy Observatory, 2 Fir Street, Black River Park, Observatory 7925, South Africa
[16]Résidence Le Dauphiné, rue Jean Bleuzen, Vanves, France
[17]Department of Physics and Astronomy, University of Sheffield, Sheffield S3 7RH, UK
[18]Instituto de Astrofísica de Canarias, E-38205 La Laguna, Tenerife, Spain
[19]NASA Goddard Space Flight Center, Greenbelt, MD 20771, USA
[20]Department of Astronomy, University of Maryland, College Park, MD 20742, USA
[21]Anton Pannekoek Institute for Astronomy, University of Amsterdam, Science Park 904, 1098 XH Amsterdam, The Netherlands
[22]Astronomy and Astrophysics Group, Department of Physics, University of Warwick, Coventry CV4 7AL, UK
[23]Department of Physics, McGill University, 3600 rue University, Montréal, QC H3A 2T8, Canada
[24]McGill Space Institute, McGill University, 3550 rue University, Montréal, QC H3A 2A7, Canada
[25]New York University Abu Dhabi, P.O. Box 129188, Abu Dhabi, UAE
[26]Eureka Scientific, Inc. 2452 Delmer Street Suite 100 Oakland, CA 94602-3017, USA
[27]National Astronomical Research Institute of Thailand (Public Organization), 260 Moo 4, T. Donkaew, A. Maerim, Chiang Mai, 50180, Thailand

ABSTRACT

We report the discovery of 1.97 ms-period gamma-ray pulsations from the 75-minute orbital-period binary pulsar now named PSR J1653−0158. The associated *Fermi*-Large Area Telescope gamma-ray source 4FGL J1653.6−0158 has long been expected to harbor a binary millisecond pulsar. Despite the pulsar-like gamma-ray spectrum and candidate optical/X-ray associations – whose periodic brightness modulations suggested an orbit – no radio pulsations had been found in many searches. The pulsar was discovered by directly searching the gamma-ray data using the GPU-accelerated *Einstein@Home* distributed volunteer computing system. The multi-dimensional parameter space was bounded by positional and orbital constraints obtained from the optical counterpart. More sensitive analyses of archival and new radio data using knowledge of the pulsar timing solution yield very stringent upper limits on radio emission. Any radio emission is thus either exception-

Corresponding author: L. Nieder
lars.nieder@aei.mpg.de

ally weak, or eclipsed for a large fraction of the time. The pulsar has one of the three lowest inferred surface magnetic-field strengths of any known pulsar with $B_{\text{surf}} \approx 4 \times 10^7$ G. The resulting mass function, combined with models of the companion star's optical light curve and spectra, suggest a pulsar mass $\gtrsim 2 M_\odot$. The companion is light-weight with mass $\sim 0.01 M_\odot$, and the orbital period is the shortest known for any rotation-powered binary pulsar. This discovery demonstrates the *Fermi*-Large Area Telescope's potential to discover extreme pulsars that would otherwise remain undetected.

Keywords: gamma rays: stars — pulsars: individual (PSR J1653−0158)

1. INTRODUCTION

The *Fermi* Large Area Telescope (LAT) source 4FGL J1653.6−0158 is a bright gamma-ray source, and the brightest remaining unassociated source (Saz Parkinson et al. 2016). It was first seen by the Energetic Gamma Ray Experiment Telescope (EGRET, Hartman et al. 1999), and was also listed in the LAT Bright Gamma-ray source list (Abdo et al. 2009) more than a decade ago. While pulsars were discovered in several other sources from this list (see, e.g., Ransom et al. 2011), the origin of 4FGL J1653.6−0158 remained unidentified. The detection of a variable X-ray and optical candidate counterpart with 75 min-period consistent with the gamma-ray position of 4FGL J1653.6−0158 provided strong evidence of it being a binary gamma-ray pulsar (Kong et al. 2014; Romani et al. 2014).

To identify the neutron star in 4FGL J1653.6−0158, we carried out a binary-pulsar search of the gamma rays, using the powerful GPU-accelerated distributed volunteer computing system *Einstein@Home*. Such searches are very computationally demanding, and would take decades to centuries on a single computer while still taking weeks or months on *Einstein@Home*. Thus, the search methods are specifically designed to ensure efficiency (Nieder et al. 2020). One key element is the use of constraints derived from optical observations. The companion's pulsar-facing side is heated by the pulsar wind, leading to a periodically varying optical light curve. This permits the orbital period P_{orb} and other orbital parameters to be tightly constrained (for a feasible search the uncertainty ΔP_{orb} needs to be less than a few milliseconds). In addition, because the sky position of the optical source is typically known to high precision (sub-milliarcsecond level), a search over position parameters is not needed.

Here we present the discovery and analysis of gamma-ray pulsations from PSR J1653−0158 in 4FGL J1653.6−0158. The pulsar is spinning very rapidly, at a rotational frequency of 508 Hz. The inferred surface magnetic-field strength is one of the lowest of all known pulsars. The discovery also confirms the 75 min orbital period. This very short orbital period raises interesting questions about the evolutionary path which created the system.

The paper is organized as follows. In Section 2, we describe the gamma-ray search, detection and analysis within LAT data. The optical analysis of the pulsar's companion, ra-

dio pulsation searches, and a continuous gravitational-wave follow-up search are presented in Section 3. We discuss the results and conclude in Section 4.

2. GAMMA-RAY PULSATIONS

2.1. *Data preparation*

We searched for gamma-ray pulsations in the arrival times of photons observed by the *Fermi* LAT (Atwood et al. 2009) between August 3, 2008 and April 16, 2018 (MJDs 54,681 and 58,224). We included SOURCE-class photons according to the P8R2_SOURCE_V6 (Atwood et al. 2012) instrument response functions (IRFs)[1], with reconstructed incidence angles within a 5° region-of-interest (RoI) around the putative pulsar position, energies above 100 MeV and zenith angles below 90°. Here, we used the presumptive companion's position as reported in the *Gaia* DR2 Catalog (hereafter *Gaia* catalog; Gaia Collaboration et al. 2018). The celestial parameters (J2000.0) are $\alpha = 16^{\text{h}}53^{\text{m}}38.05381(5)$ and $\delta = -01°58'36''8930(5)$, with 1$\sigma$ uncertainties on the last digits reported in parentheses.

Using the photon incidence angles and energies, we constructed a probability or weight for each photon, $w_j \in [0, 1]$, where j labels the photon: w_j is the probability that the jth photon originated from the posited source, as opposed to a fore- or background source. These weights were computed by gtsrcprob, using the preliminary *Fermi*-LAT 8-year source catalog[2] as a model for the flux within the RoI without performing a full spectral fit. Weighting the contribution of each photon to a detection statistic in this way greatly increases the search sensitivity (Kerr 2011), and the distribution of weights can be used to predict expected signal-to-noise ratios (Nieder et al. 2020).

The data set used here consisted of $N = 354,009$ photons, collected over a period of 3,542 days. The properties of the detection statistics (semicoherent power S_1, coherent power P_1, and H statistic) depend upon the lowest moments of the weights, which are

$$\sum_{j=1}^{N} w_j \approx 10266, \ \sum_{j=1}^{N} w_j^2 \approx 2464, \text{ and } \sum_{j=1}^{N} w_j^4 \approx 931.$$

[1] See https://fermi.gsfc.nasa.gov/ssc/data/analysis/LAT_essentials.html
[2] https://fermi.gsfc.nasa.gov/ssc/data/access/lat/fl8y/

These moments determine the ultimate sensitivity to a particular pulse profile and pulsed fraction, as given in Eq. (11) in Nieder et al. (2020).

Following the pulsar discovery, we extended this dataset to February 23, 2020 (MJD 58,902), using the latest `P8R3_SOURCE_V2` IRFs (Bruel et al. 2018), a larger maximum zenith angle of 105°, and using the *Fermi*-LAT Fourth Source Catalog (hereafter 4FGL, Abdollahi et al. 2020) as the RoI model for the photon probability weight computations.

2.2. *Search*

The binary-pulsar search methods are described by Nieder et al. (2020), which are a generalization and extension of the isolated-pulsar search methods from Pletsch & Clark (2014).

The searched ranges are guided by the known millisecond pulsar (MSP) population in the Australia Telescope National Facility (ATNF) Pulsar Catalogue[3] (Manchester et al. 2005). For the spin frequency, we searched $f \in [0, 1500]$ Hz[4]. The spin-frequency derivative was expected to be in the range $\dot{f} \in [-10^{-13}, 0]$ Hz s^{-1}.

The sky position of the candidate optical counterpart is constrained to high precision in the *Gaia* catalog, so no astrometric search is required. The proper motion measured by *Gaia* for the optical counterpart was ignored for the search.

2.2.1. *Orbital Constraints from Optical Observations*

The orbital period estimate of Romani et al. (2014) was derived from Southern Astrophysical Research (SOAR), WIYN and Catalina Sky Survey (CSS) observations. These were augmented by new 350s SOAR Goodman High Throughput Spectrograph (GHTS) g', r', i' exposures (63 g', 75 r', 42 i') from MJD 56,514.074 – 56,516.184, and with the 300 s g', r' and i' exposures obtained by Kong et al. (2014) using the Wide Field camera (WFC) on the 2.5m Isaac Newton Telescope (INT) on La Palma. For these two data sets, the scatter about the light curve trends was appreciably larger than the very small statistical errors; we thus add 0.03 mag in quadrature to account for unmodeled fast variability and/or photometry systematics. To further refine the orbital period uncertainty, we obtained additional observations in u', g' and i' using the high-speed multi-band imager ULTRACAM (Dhillon et al. 2007) on the 4.2m William Herschel Telescope (WHT) on two nights (MJDs 57,170 and 57,195), covering six and three orbits of the binary system, respectively, with a series of 20 s exposures. Conditions were very poor on the first night with seeing > 5 arcsec, particularly at the beginning of the

observation. We therefore only used the second night's data for the optical light curve modeling in Section 3.1, adding the latter half of the first night's observations for orbital period estimation. Finally, we obtained further INT+WFC exposures (23 g', 151 r', 45 i') on MJD 57,988 – 57,991. The g', r', i' filter fluxes were referenced to in-field PanSTARRS catalog sources, and then converted to the SDSS scale. The u' photometry was calibrated against an SDSS standard star observed on MJD 57,170. We estimate ∼ 0.05 mag systematic uncertainties in g', r' and i', with uncertainties as large as ∼ 0.1 mag in u'.

We constrained the orbital period using the multi-band Lomb Scargle periodogram method (VanderPlas & Ivezić 2015, excluding the u' ULTRACAM data, as the modulation has very low signal-to-noise ratio in this band). To infer reasonable statistical uncertainties, we fit for and removed constant magnitude offsets, consistent with our estimated calibration uncertainties, between each night's observations in each band, and additionally rescaled the magnitude uncertainties to obtain a reduced chi-square of unity. This constrained the orbital period to $P_{\mathrm{orb}} = 0.0519447518 \pm 6.0 \times 10^{-9}$ days, where the quoted uncertainty is the 1σ statistical uncertainty. For the pulsation search, we chose to search the 3σ range around this value.

In Romani et al. (2014), the time of the pulsar's ascending node, T_{asc}, was estimated from the photometric light curve. However, the optical maximum is distinctly asymmetric (see Section 3.1), which can bias orbital phase estimates. We therefore used the spectroscopic radial velocity measurements from Romani et al. (2014), folded at the orbital period obtained above, and fit the phase of a sinusoidal radial velocity curve, finding $T_{\mathrm{asc}} = \mathrm{MJD}\,56513.47981 \pm 2.1 \times 10^{-4}$. However, as radial velocities may still be slightly biased by asymmetric heating, we elected to search a wide range around this value, corresponding to $\pm 8\sigma$.

For the projected semimajor-axis parameter $x = a_1 \sin i/c$, we decided to start searching $x \in [0, 0.1]$ s, with the intention to go to larger values in the case of no detection. For a pulsar mass of $1.6 M_\odot$, this would cover the companion mass range up to $0.2 M_\odot$ and would include companion masses of all known "black-widow" systems as well as some of the lower mass "redback" systems (Roberts 2013; Strader et al. 2019). Here, a_1 is the Die kpulsar's semimajor axis, i denotes the inclination angle, and c the speed of light. As described in Nieder et al. (2020), we expected $x \in [0, 0.2]$ s based on the companion's velocity amplitude reported by Romani et al. (2014) and the masses expected for "spider" companions, i.e. black-widow or redback companions.

2.2.2. *Search grids*

To cover the relevant orbital-parameter space in $\{x, P_{\mathrm{orb}}, T_{\mathrm{asc}}\}$, we use *optimized grids* (Fehrmann & Pletsch

---

[3] http://www.atnf.csiro.au/research/pulsar/psrcat

[4] The upper limit has been chosen to be sensitive to pulsars spinning at up to 750 Hz, which have two-peaked pulse profiles where the peaks are half a rotation apart (see also, Pletsch & Clark 2014). Note that the current record spin frequency is 716 Hz (Hessels et al. 2006).

2014). These grids use as few points as possible still ensuring that a signal within the relevant space should be detected. Furthermore, they are able to cover the orbital-parameter space efficiently even though the required density depends on one of the orbital parameters, x.

Key to building an optimized grid is to know how the signal-to-noise ratio drops due to offsets from the true pulsar parameters. This is estimated using a *distance metric* on the orbital-parameter space (Nieder et al. 2020). In our case, the three-dimensional grid was designed to have a worst-case mismatch $\bar{m} = 0.2$, i.e. not more than 20% of the (semicoherent or coherent) signal power should be lost due to orbital-parameter offsets. Of most relevance is that 99% of randomly injected orbital-parameter points have a mismatch below $\bar{m} = 0.04$ to the closest grid point.

Due to the f-dependency of the required grid-point density, we search f in steps, and build the corresponding orbital grids prior to the start of the search on the computing cluster ATLAS in Hannover (Aulbert & Fehrmann 2008).

2.2.3. *Einstein@Home*

Searching the 5-dimensional parameter space $\{f, \dot{f}, x, P_{orb}, T_{asc}\}$ is a huge computational task with over 10^{17} trials. Thus, the first (computing-intensive) search stages were performed on *Einstein@Home*, a distributed volunteer computing system (Allen et al. 2013). As done for radio pulsar searches previously, the search code utilizes the approximately 10,000 GPUs active on *Einstein@Home* for a computing speed-up of ~ 10, comparing the runtimes on CPUs and GPUs.

The parameter space is divided into more than one million regions. Searching one of these is called a "work unit". These work units are sent to computers participating in *Einstein@Home*, and are searched when the computer is otherwise idle. Depending on the system, searching a work unit takes between half an hour and up to a few hours of computational time. In total, the search would have taken more than 50 years on a single computer, but using *Einstein@Home* it took less than two weeks.

2.2.4. *Gamma-ray detection*

The search process involves multiple stages in which semicoherent statistics are constructed, and the most significant candidates are passed on to fully coherent follow-up stages (for full details of the search pipeline and signal-to-noise ratio definitions, see Nieder et al. 2020). In the last semicoherent stage, a candidate found at a frequency of 1016 Hz had signal-to-noise ratio $S_1 = 8.6$, which we now associate with PSR J1653−0158. This was not the strongest candidate or far above the background of noise, but was among the ten most significant candidates in its work unit, and therefore passed on to the coherent stage. In the coherent stage, it was very significant, with signal-to-noise ratio $P_1/2 = 94$.

The search follow-ups confirmed significant pulsations with period $P \approx 1.97$ ms (or $f \approx 508$ Hz), while the actual search revealed an alias at twice the pulsar frequency. This may be because the signal has significant power in the second harmonic.

Note that the signal was found outside the 3σ range in T_{asc} from the constraints reported in this work, and outside the 3σ range given by Romani et al. (2014). This can be caused by asymmetric heating (see Section 2.2.1).

2.3. *Timing*

The parameters used in the phase model to describe the pulsar's rotation are measured in a timing analysis. We use the timing methods as explained in Clark et al. (2017), which are an extension of the methods by Kerr et al. (2015). The basic principle is that the parameter space around the discovery parameters is explored using a Monte Carlo sampling algorithm with a template pulse profile.

To marginalize over the pulse profile template, we vary the template parameters as described in Nieder et al. (2019). In the case of PSR J1653−0158, we used a template consisting of two symmetrical, wrapped Gaussian peaks. We used constraints on the peaks' full-width at half maximum, such that the peaks must be broader than 5% of a rotation, and narrower than half a rotation.

Our timing solution over 11 years of LAT data is shown in Table 1. The folded gamma-ray data and the pulse profile are portrayed in Fig. 1.

The observed spin-down $\dot{P}$ is one of the lowest of all known pulsars. To estimate the intrinsic $\dot{P}$ we account for the Shklovskii effect (Shklovskii 1970), and the Galactic acceleration (see, e.g., Damour & Taylor 1991). The results are summarized in Table 1. The observed contribution due to the difference in Galactic acceleration of the Sun and the pulsar is computed with $R_{Sun} = 8.21$ kpc, $z_{Sun} = 14$ pc, and the Galactic potential model `PJM17_best.Tpot` (McMillan 2017), as implemented in their code[5]. For PSR J1653−0158, we used $R_{J1653} = 7.48$ kpc, and $z_{J1653} = 367$ pc, assuming $d = 840$ pc (see Table 2). The contributions parallel and perpendicular to the Galactic disk nearly cancel each other, so that the choice of the potential and its relevant parameters have a seemingly large effect on the actual small value of $\dot{P}_{Gal}$, and can even change the sign. However, the overall kinematic contribution to the observed $\dot{P}$ is dominated by the Shklovskii term, and its uncertainty by the uncertainty in the distance estimate. The estimated intrinsic spin-down is $\dot{P}_{int} = 8.5 \times 10^{-22}$ s s^{-1} for distance $d = 840$ pc.

3. MULTIWAVELENGTH & MULTIMESSENGER

---

[5] https://github.com/PaulMcMillan-Astro/GalPot

Table 1. Timing solution for PSR J1653−0158.

Parameter	Value
Range of observational data (MJD)	54682 – 58902
Reference epoch (MJD)	56100.0
Celestial parameters from Gaia catalog	
R.A., α (J2000.0)	$16^h53^m38\overset{s}{.}05381(5)$
Decl., δ (J2000.0)	$-01°58'36\overset{''}{.}8930(5)$
Positional epoch (MJD)	57205.875
Proper motion in R.A., $\mu_\alpha \cos\delta$ (mas yr^{-1})	-19.62 ± 1.86
Proper motion in Dec., μ_δ (mas yr^{-1})	-3.74 ± 1.12
Parallax[a], ϖ (mas)	1.88 ± 1.01
Timing parameters	
Spin frequency, f (Hz)	508.21219457426(6)
Spin-frequency derivative, $\dot{f}$ (Hz s^{-1})	$-6.204(8) \times 10^{-16}$
Spin period, P (ms)	1.9676820247057(2)
Spin-period derivative, $\dot{P}$ (s s^{-1})	$2.402(3) \times 10^{-21}$
Proj. semimajor axis, x (s)	0.01071(1)
Orbital period, P_{orb} (days)	0.0519447575(4)
Epoch of ascending node, T_{asc} (MJD)	56513.479171(8)
Derived parameters for distance $d = 840$ pc	
Shklovskii spin down, $\dot{P}_{Shk}$ (s s^{-1})	1.6×10^{-21}
Galactic acceleration spin down, $\dot{P}_{Gal}$ (s s^{-1})	-4.8×10^{-23}
Spin-down power, $\dot{E}$ (erg s^{-1})	4.4×10^{33}
Surface B-field, B_{surf} (G)	4.1×10^7
Light-cylinder B-field, B_{LC} (G)	5.0×10^4
Characteristic age, τ_c (Gyr)	37
Gamma-ray luminosity[b], L_γ (erg s^{-1})	2.9×10^{33}
Gamma-ray efficiency, $n_\gamma = L_\gamma/\dot{E}$	0.66

NOTE— The JPL DE405 solar system ephemeris has been used and times refer to TDB.

[a] Corresponds to a model independent distance $d = 533^{+625}_{-187}$ pc, but for the derived parameters the consistent distance $d = 840^{+40}_{-40}$ pc derived from optical modeling is used (see Table 2).

[b] Taken from 4FGL Source Catalog (Abdollahi et al. 2020).

3.1. *Optical Light Curve Modeling and System Masses*

By modeling the optical light curves and radial velocities we can constrain the binary mass and distance and the system viewing angle. Comparing the individual filters between nights suggest small $\delta m \approx 0.05$ shifts in zero points, consistent with the systematic estimates above. Correcting to match the individual filters, we then re-binned the light curve,
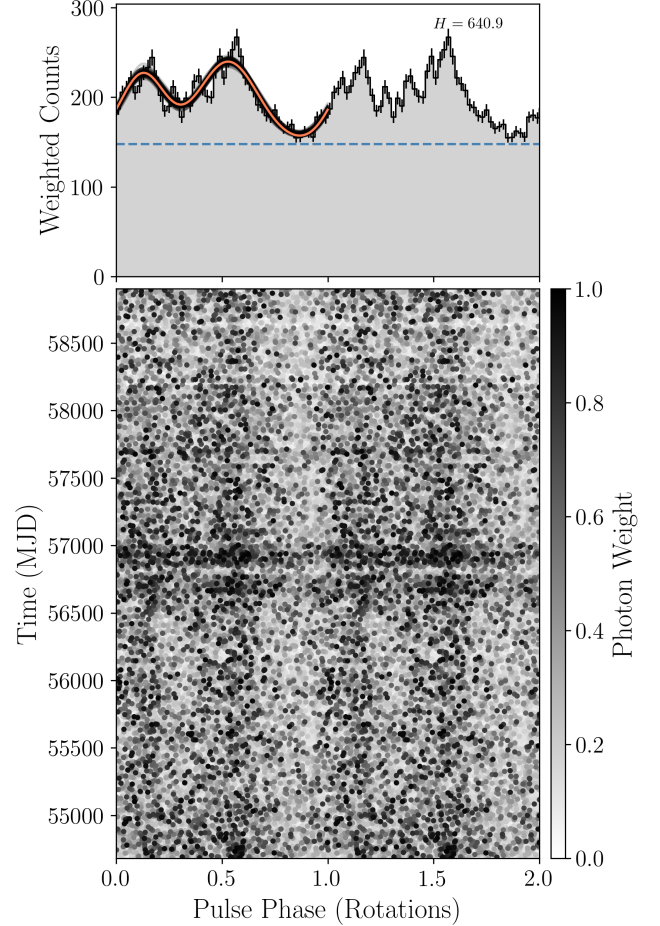
Figure 1. Integrated pulse profile and phase-time diagram of PSR J1653−0158, showing two identical rotations. Top: The histogram shows the weighted counts for 50 bins. The orange curve indicates the pulse-profile template with the highest signal power, and the transparent black curves represent 100 templates randomly selected from the Monte Carlo samples after the chain stabilized, to indicate the uncertainty on the profile. The dashed blue line denotes the source background. Bottom: Each point represents the pulsar's rotational phase at emission of a photon, with the intensity indicating the photon's probability weight. Note that PSR J1653−0158 received more exposure between MJDs 56,600 and 57,000 when the LAT pointed more often towards the Galactic center.

placing the photometry on a regular grid with points spaced by $\delta\phi = 0.004$, using the Python package `Lightkurve`; after excision of a few obviously discrepant points, we retain 248 u', 239 g', 220 r' and 245 i' points for light curve fitting (Fig. 2). This fitting is done with a version of the `Icarus` code of Breton et al. (2013) modified to include the effect of hot spots on the companion surface, likely generated by precipitation of particles from the intrabinary shock (IBS) to companion magnetic poles (Sanchez & Romani 2017). All parameter values and errors are determined by MCMC modeling.
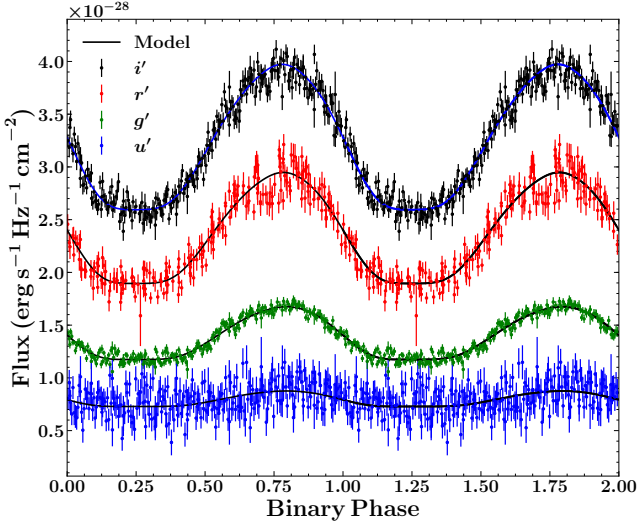
Figure 2. u', g', r', and i' light curves for PSR J1653−0158, with the best-fit model curves. Note the flat minima and decreasing modulation for bluer colors, a consequence of the hard spectrum veiling flux. Two identical cycles are shown for clarity.

The very shallow modulation of these light curves might normally be interpreted as indicating a small inclination i. However given the large companion radial velocity amplitude $K = 666.9 \pm 7.5\,\mathrm{km\,s^{-1}}$, implying a mass function $f(M) = 1.60 \pm 0.05\,M_\odot$, measured by Romani et al. (2014), a small inclination would give an unphysical, large neutron star mass. As noted in that paper, the light curves and spectra show that a strong blue non-thermal veiling flux dominates at orbital minimum. With increasingly shallow modulation for the bluer colors, this is also evident in the present photometry. Thus the minimal model for this pulsar must include a non-thermal veiling flux. Although this is likely associated with the IBS, we model it here as a simple power law with form $f_\nu = f_A (\nu/10^{14}\,\mathrm{Hz})^{-p}$. This flux is nearly constant through the orbit, although there are hints of phase structure, e.g. in r' and i' at $\phi_B = 0.72$ (see Fig. 2). Any model without such a power law component is completely unacceptable. These fits prefer an A_V slightly higher than, but consistent with the maximum in this direction (obtained by $\sim 300\,\mathrm{pc}$; Green et al. 2019)[6].

In Fig. 2, one notices that the orbital maximum is slightly delayed from $\phi_B = 0.75$, especially in the bluer colors. Such asymmetric heating is most easily modeled adding a polar hot spot with location (θ_c, ϕ_c) and local temperature increase A_c in a Gaussian pattern of width σ_c; when we include such a component, the fit improves greatly, with $\Delta\chi^2/\mathrm{DoF} = -0.34$. The Akaike Information Criterion comparison of the two models indicates that the model with a hot spot is preferred at

[6] https://doi.org/10.7910/DVN/2EJ9TX

Table 2. Light curve fit results for PSR J1653−0158. Parameters from the best-fit light curve/radial velocity models, with and without a surface hot spot, including MCMC errors.

Parameters	Veiled	Veiled+HS
Inclination, i (deg)	$79.4^{+5.7}_{-6.8}$	$72.3^{+5.0}_{-4.9}$
Filling factor, f_c	$0.97^{+0.02}_{-0.02}$	$0.88^{+0.03}_{-0.03}$
Heating luminosity, L_P ($10^{33}\,\mathrm{erg\,s^{-1}}$)	$3.33^{+0.39}_{-0.34}$	$3.15^{+0.26}_{-0.27}$
Night-side temperature, T_N (K)	3250^{+243}_{-331}	3295^{+227}_{-300}
V-band extinction, A_V	$1.06^{+0.08}_{-0.10}$	$1.06^{+0.07}_{-0.09}$
Distance, d (pc)	830^{+50}_{-50}	840^{+40}_{-40}
Veiling flux norm, f_A (μJy)	$101.7^{+11.4}_{-11.1}$	$99.9^{+11.7}_{-11.4}$
Veiling flux index, p	$0.50^{+0.05}_{-0.03}$	$0.49^{+0.03}_{-0.03}$
Spot azimuth, θ_c (deg)	...	$286.8^{+5.8}_{-6.9}$
Spot co-latitude, ϕ_c (deg)	...	$-50.5^{+9.2}_{-8.4}$
Gaussian spot width, σ_c (deg)	...	$25.2^{+5.0}_{-4.9}$
Spot temperature increase, A_c	...	$0.66^{+0.21}_{-0.21}$
Neutron-star mass, M_{NS} ($M_\odot$)	$1.99^{+0.18}_{-0.08}$	$2.17^{+0.21}_{-0.15}$
Companion mass, M_c ($M_\odot$)	$0.013^{+0.001}_{-0.001}$	$0.014^{+0.001}_{-0.001}$
χ^2/DoF	1.72	1.38

the 10^{-18} level, despite the extra degrees of freedom. We give the fit parameters for both models in Table 2. Note that with the fine structure near maximum, the model is not yet fully acceptable ($\chi^2/\mathrm{DoF} \sim 1.4$). More detailed models, including direct emission from the IBS or possibly the effects of companion global winds (Kandel & Romani 2020), may be needed to fully model the light curves. Such modeling would be greatly helped by light curves over an even broader spectral range, with IBS effects increasingly dominant in the UV, and low temperature companion emission better constrained in the IR. With many cycles we could also assess the reality (and stability) of the apparent fine structure and test for hot spot motion.

Our fit distance may be cross-checked with two other quantities. (1) With the 4FGL energy flux $f_\gamma = 3.5 \times 10^{-11}\,\mathrm{erg\,cm^{-2}\,s^{-1}}$ between 100 MeV and 100 GeV, our fit distance gives an isotropic gamma-ray luminosity $L_\gamma = 3 \times 10^{33}\,\mathrm{erg\,s^{-1}}$, in good agreement with the $L_\gamma \approx (10^{33}\,\mathrm{erg\,s^{-1}}\dot{E})^{1/2}$ heuristic luminosity law (Abdo et al. 2013), as a function of the spin-down power $\dot{E}$. This luminosity is consistent with the model for direct radiative heating of the companion. (2) Our fit distance is also consistent with the model-independent, but lower accuracy, distance from the *Gaia* parallax. Thus, the 840 pc distance seems reliable, although systematic effects probably dominate over the rather small $\sim 50\,\mathrm{pc}$ statistical errors.

Armed with the fits, we can estimate the companion masses, correcting the observed radial velocity amplitude

(fit with a K-star template) for the temperature-dependent weighting of the absorption lines across the companion face as in Kandel & Romani (2020). The results indicate substantial mass accretion, as expected for these ultra-short period systems. With the preferred Veiled+HS model the mass significantly exceeds $2.0 M_{\odot}$, adding to the growing list of spider binaries in this mass range. Note that the inclination i uncertainty dominates the error in this mass determination. Broader range photometric studies, with better constraint on the heating pattern, can reduce the i uncertainty.

3.2. *Radio pulsation searches*

The pulsar position has been observed in radio multiple times. Several searches were performed before the gamma-ray pulsation discovery, and a few very sensitive follow-up searches afterwards. Despite the more than 20 observations with eight of the most sensitive radio telescopes, no radio pulsations have been found.

The results of the radio searches are given in Table 3. Observations are spread over 11 years, with observing frequencies ranging from 100 MHz up to 5 GHz. All orbital phases have been covered by most of the telescopes. Since there was no detection, the table also gives upper limits derived from the observations. For all but LOFAR, the data (both archival and recent) was folded with the gamma-ray-derived ephemeris, and searched only over dispersion measure.

The strictest upper limits on pulsed radio emission are $8\,\mu$Jy at $1.4\,$GHz, and $20\,\mu$Jy at $4.9\,$GHz. This is fainter than the threshold of $30\,\mu$Jy that Abdo et al. (2013) use to define a pulsar to be "radio quiet". Note, that for the calculation of the limits we included the parts of the orbit where eclipses might be expected for spider pulsars. Thus, the limit constrains the maximum emission of the system, and not the maximum emission from the pulsar alone.

3.3. *Continuous gravitational waves*

We search for nearly monochromatic, continuous gravitational waves (GWs) from PSR J1653−0158, using data from the first[7] and second[8] observing runs of the Advanced LIGO detectors (The LIGO Scientific Collaboration et al. 2019). We assume that GWs are emitted at the first and second harmonic of the neutron star's rotational frequency, as would occur if the spin axis is misaligned with the principal axes of the moment of inertia tensor (Jones 2010, 2015).

We employ two different analysis procedures, which yield consistent results. The first is frequentist, based on the multidetector maximum-likelihood $\mathcal{F}$-statistic introduced by Cutler & Schutz (2005). The second is the Bayesian time-domain method (Dupuis & Woan 2005) as detailed by Pitkin

[7] https://doi.org/10.7935/K57P8W9D
[8] https://doi.org/10.7935/CA75-FM95

et al. (2017), with triaxial non-aligned priors (Pitkin et al. 2015). Both methods coherently combine data from the two detectors, taking into account their antenna patterns and the GW polarization. The $\mathcal{F}$-statistic search excludes data taken during times when the relevant frequency bands are excessively noisy.

The results are consistent with no GW emission. At twice the rotation frequency, the $\mathcal{F}$-statistic 95% confidence upper limit on the intrinsic GW amplitude h_0 is 4.4×10^{-26}. The 95%-credible interval upper limit from the Bayesian analysis on $h_0 = 2C_{22}$ is 3.0×10^{-26}. At the rotation frequency (only checked with the Bayesian method) the 95% confidence upper limit on the amplitude C_{21} is 6.6×10^{-26}.

Since the dominant GW frequency might be mismatched from twice the rotation frequency (Abbott et al. 2019a), we performed an $\mathcal{F}$-statistic search in a ± 1 Hz band around this, with an extended $\dot{f}$-range. This yields larger upper limits on h_0, with mean value of 1.3×10^{-25} in $10\,$mHz-wide bands. Full details are given in the supplementary materials.

Our upper limits on h_0 at twice the rotation frequency may also be expressed as upper limits on the ellipticity ϵ of the pulsar (Abbott et al. 2019b). This is $\epsilon = 3.9 \times 10^{-8} \times (h_0/5 \times 10^{-26}) \times (10^{45}\text{g cm}^3/I_{zz}) \times (840\,\text{pc}/d)$, where I_{zz} is the moment of inertia about the spin axis, and d is the distance.

As is the case for most known pulsars, it is unlikely that our searches would have detected a GW signal. In fact, suppose that all of the rotational kinetic-energy losses associated with the intrinsic spin-down is via GW emission. Then assuming the canonical $I_{zz} = 10^{45}\text{g cm}^3$, this would imply a "spin-down" ellipticity $\epsilon^{\text{sd}} = 4.7 \times 10^{-10}$, which is a factor ~ 80 below our upper limit.

4. DISCUSSION & CONCLUSIONS

PSR J1653−0158 is the second binary pulsar (Pletsch et al. 2012), and the fourth MSP (Clark et al. 2018) to be discovered through periodicity searches of gamma rays. This pulsar is remarkable in many ways. It is only the second rotationally-powered MSP from which no radio pulsations have been detected. It is among the fastest-rotating known pulsars with spin frequency $f = 508$ Hz. The 75 min orbital period is shorter than for any other known rotation-powered pulsar, with the previous record being PSR J1311−3430 with a 93 min orbit (Pletsch et al. 2012). The inferred surface magnetic field is possibly the weakest, depending on the Shklovskii correction.

The discovery was enabled by constraints on the sky-position and orbital parameters from optical observations, together with efficient search techniques and the large computing power of the distributed volunteer computing system *Einstein@Home*. The detection proves that the optically variable candidate counterpart (Kong et al. 2014; Romani et al.

Table 3. Summary of radio searches for PSR J1653−0158. The columns show the telescope used, the observed frequency range, the start time and data span, the range of orbital phases covered, the resulting limit on a pulsed component, and a reference with relevant details.

Telescope	Frequency (MHz)	Data start (UTC)	Data span (s)	Orbital phase	Limit (μJy)	Reference / Survey
Effelsberg	1210–1510	2010 May 26, 21:33	1920	0.88–1.31	63	Barr et al. (2013)
Effelsberg	1210–1510	2014 Aug 26, 20:27	4600	0.15–1.17	41	
Effelsberg	4600–5100	2014 Aug 29, 18:52	4600	0.62–1.65	33	
Effelsberg	4600–5100	2020 Jun 18, 22:09	11820	0.85–3.48	20	
FAST	1050–1450	2020 Jun 04, 16:30	2036	0.80–1.25	8	Li et al. (2018)
GBT	720–920	2009 Sep 20, 00:49	3200	0.93–1.65	51	
GBT	720–920	2010 Dec 13, 21:04	1300	0.91–1.20	80	
GBT	720–920	2011 Dec 22, 12:11	2400	0.74–1.27	59	Sanpa-arsa (2016)
GBT	305–395	2012 Feb 22, 14:31	1700	0.27–0.65	301	
GBT	1700–2300	2014 Nov 18, 14:28	1200	0.36–0.63	43	
GBT	1700–2300	2014 Nov 20, 13:56	2400	0.44–0.98	30	
GBT	1700–2300	2014 Nov 21, 22:38	1800	0.66–1.07	35	
GBT	720–920	2017 Jan 28, 13:20	1200	0.97–1.24	83	
GMRT	591–623	2011 Feb 02, 02:32	1800	0.94–1.34	730	Bhattacharyya et al.
GMRT	306–338	2012 May 15, 22:31	1800	0.54–1.06	990	(2013, 2020 in prep.)
GMRT	306–338	2012 Jun 11, 17:49	1800	0.55–0.95	990	"
GMRT	591–623	2014 Aug 19, 13:44	1800	0.00–0.54	270	"
GMRT	591–623	2014 Aug 30, 11:17	1800	0.80–1.38	270	"
GMRT	591–623	2015 Dec 28, 03:55	1800	0.73–1.13	270	"
LOFAR	110–180	2017 Mar 15, 04:18	15×320	Full orbit	6,200	Bassa et al. (2017)
LOFAR	110–180	2017 Apr 15, 02:20	15×320	Full orbit	6,200	"
Lovell	1332–1732	2019 Mar 15, 01:34	5400	0.57–1.77	82	
Lovell	1332–1732	2019 Mar 16, 02:53	5400	0.87–2.08	82	
Lovell	1332–1732	2019 Mar 17, 01:47	5400	0.25–1.45	82	
Nançay	1230–1742	2014 Aug 20, 18:33	1850	0.12–0.53	77	Desvignes et al. (2013)
Parkes	1241–1497	2016 Nov 05, 06:17	3586	0.26–1.06	178	Camilo et al. (2016)

NOTE— The orbital phase is given in orbits, and ranges > 1 indicate that more than one orbit has been observed. The considered maximum dispersion measure varies with the observing frequency from DM = 80 pc cm^{-3} at the lowest frequencies to DM = 350 pc cm^{-3} at the highest frequencies. To estimate the limit on the pulsed component, we used Eq. (6) from Ray et al. (2011) assuming a pulse width of $0.25\,P$, and a threshold signal-to-noise ratio S/N$_{\mathrm{min}}$ = 7.

2014) is indeed the black-widow-type binary companion to PSR J1653−0158, and it conclusively resolves the nature of the brightest remaining unidentified gamma-ray source, first found more than two decades ago (Hartman et al. 1999).

The distance to PSR J1653−0158, and its proper motion are well constrained. *Gaia* measurements of the parallax, $\varpi = 1.88 \pm 1.01$ mas, imply a distance $d = 530^{+470}_{-200}$ pc. A consistent, but tighter constraint is given by our optical modeling with $d = 840^{+40}_{-40}$ pc. The proper motion (see Table 1) is also measured with good precision (*Gaia* and our timing are in agreement).

PSR J1653−0158 has one of the lowest observed spin-period derivatives of all known pulsars ($\dot{P} = 2.4 \times 10^{-21}$ s s^{-1}). The intrinsic $\dot{P} = 8.5 \times 10^{-22}$ s s^{-1} (accounting for Galactic ac-

celeration and Shklovskii effects) is even smaller. In Fig. 3, PSR J1653−0158 is shown in a P-$\dot{P}$ diagram, alongside the known radio and gamma-ray pulsar population outside of globular clusters.

The intrinsic $\dot{P}$ can be used to estimate the pulsar's spin-down power $\dot{E}$, surface magnetic-field strength B_{surf}, magnetic-field strength at the light cylinder B_{LC}, and characteristic age τ_{c}. These are given in Table 1 for $d = 840$ pc. Constant lines of $\dot{E}$, B_{surf}, and τ_{c} are displayed in Fig. 3 to show the distance-dependent ranges.

Spider pulsars in very-short-period orbits are difficult to discover with traditional radio searches. Even though we can now fold the radio data with the exact parameters, PSR J1653−0158 is still not visible. There are two simple
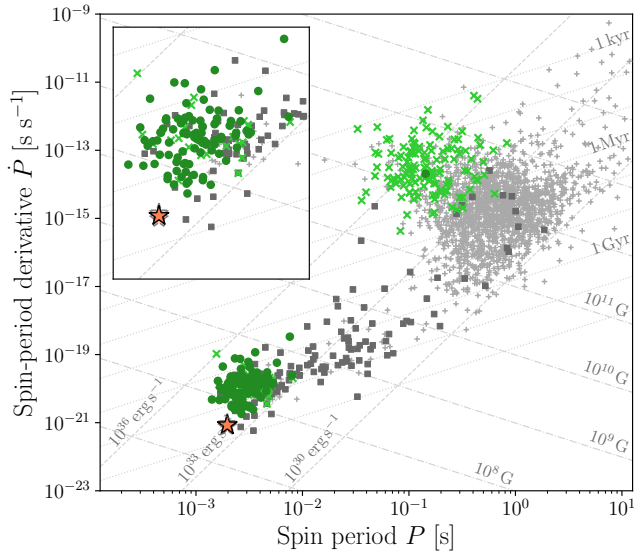
Figure 3. Newly detected PSR J1653−0158 on a P-$\dot{P}$ diagram of the known pulsar population outside of globular clusters. The MSP population is shown magnified in the inset. LAT pulsars are marked in green (isolated by a cross and binary by a circle). Non-LAT pulsars in the ATNF are marked in gray (isolated by a plus and binary by a square). The lines show constant surface magnetic-field strength (dashed-dotted), characteristic age (dotted), and spin-down power (dashed). The spin period and intrinsic spin-period derivative of PSR J1653−0158 are marked by the orange star. The transparent stars indicate the (distance-dependent) maximum and minimum intrinsic spin-period derivative according to the distance estimated from our optical models.

explanations for the non-detection of radio pulsations. (1) PSR J1653−0158 is intrinsically radio-quiet, in that its radio beam does not cross the line-of-sight, or it has a very low luminosity. There is one other radio quiet MSP known (Clark et al. 2018). (2) Radio emission is blocked by material produced by the pulsar evaporating its companion.

The minimum average density of the companion $64 \, \mathrm{g\,cm^{-3}}$ is very high, assuming a filled Roche lobe (Eggleton 1983). Using the filling factor from optical modeling, the average companion density $73 \, \mathrm{g\,cm^{-3}}$ is even higher. The high density and the compact orbit suggest that the companion may be a helium white dwarf remnant, and that the system may have evolved from an ultracompact X-ray binary (Sengar et al. 2017; Kaplan et al. 2018).

The discovery of PSR J1653−0158 is the result of a multiwavelength campaign. The pulsar-like gamma-ray spectrum, and the non-detection of radio pulsations, motivated the search for a visible companion. This was subsequently discovered in optical and X-ray observations. Further optical observations provided constraints on the orbital parameters which were precise enough to enable a successful gamma-ray pulsation search.

REFERENCES

Abbott, B. P., Abbott, R., Abbott, T. D., et al. 2019a, PhRvD, 99, 122002, doi: 10.1103/PhysRevD.99.122002

—. 2019b, ApJ, 879, 10, doi: 10.3847/1538-4357/ab20cb

Abdo, A. A., Ackermann, M., Ajello, M., et al. 2009, ApJS, 183, 46, doi: 10.1088/0067-0049/183/1/46

Abdo, A. A., Ajello, M., Allafort, A., et al. 2013, ApJS, 208, 17, doi: 10.1088/0067-0049/208/2/17

Abdollahi, S., Acero, F., Ackermann, M., et al. 2020, ApJS, 247, 33, doi: 10.3847/1538-4365/ab6bcb

Allen, B., Knispel, B., Cordes, J. M., et al. 2013, ApJ, 773, 91, doi: 10.1088/0004-637X/773/2/91

Astropy Collaboration, Robitaille, T. P., Tollerud, E. J., et al. 2013, A&A, 558, A33, doi: 10.1051/0004-6361/201322068

Astropy Collaboration, Price-Whelan, A. M., Sipőcz, B. M., et al. 2018, AJ, 156, 123, doi: 10.3847/1538-3881/aabc4f

Atwood, W., Albert, A., Baldini, L., et al. 2012, in Proceedings of the 4th Fermi Symposium, ed. T. J. Brandt, N. Omodei, & C. Wilson-Hodge, eConf C121028, 8

Atwood, W. B., Abdo, A. A., Ackermann, M., et al. 2009, ApJ, 697, 1071, doi: 10.1088/0004-637X/697/2/1071

Aulbert, C., & Fehrmann, H. 2008, Forschungsbericht 2008 - Max-Planck-Institut für Gravitationsphysik, Teilinstitut Hannover, https://www.mpg.de/308429/forschungsSchwerpunkt

Barr, E. D., Guillemot, L., Champion, D. J., et al. 2013, MNRAS, 429, 1633, doi: 10.1093/mnras/sts449

Bassa, C. G., Pleunis, Z., Hessels, J. W. T., et al. 2017, ApJL, 846, L20, doi: 10.3847/2041-8213/aa8400

Bhattacharyya, B., Roy, J., Ray, P. S., et al. 2013, ApJL, 773, L12, doi: 10.1088/2041-8205/773/1/L12

Breton, R. P., Rappaport, S. A., van Kerkwijk, M. H., & Carter, J. A. 2012, ApJ, 748, 115, doi: 10.1088/0004-637X/748/2/115

Breton, R. P., van Kerkwijk, M. H., Roberts, M. S. E., et al. 2013, ApJ, 769, 108, doi: 10.1088/0004-637X/769/2/108

Bruel, P., Burnett, T. H., Digel, S. W., et al. 2018, arXiv e-prints, arXiv:1810.11394. https://arxiv.org/abs/1810.11394

Camilo, F., Reynolds, J. E., Ransom, S. M., et al. 2016, ApJ, 820, 6, doi: 10.3847/0004-637X/820/1/6

Clark, C. J., Wu, J., Pletsch, H. J., et al. 2017, ApJ, 834, 106, doi: 10.3847/1538-4357/834/2/106

Clark, C. J., Pletsch, H. J., Wu, J., et al. 2018, Science Advances, 4, eaao7228, doi: 10.1126/sciadv.aao7228

Cutler, C., & Schutz, B. F. 2005, PhRvD, 72, 063006, doi: 10.1103/PhysRevD.72.063006

Damour, T., & Taylor, J. H. 1991, ApJ, 366, 501, doi: 10.1086/169585

Desvignes, G., Cognard, I., Champion, D., et al. 2013, in IAU Symposium, Vol. 291, Neutron Stars and Pulsars: Challenges and Opportunities after 80 years, ed. J. van Leeuwen, 375–377, doi: 10.1017/S1743921312024179

Dhillon, V. S., Marsh, T. R., Stevenson, M. J., et al. 2007, MNRAS, 378, 825, doi: 10.1111/j.1365-2966.2007.11881.x

Dupuis, R. J., & Woan, G. 2005, PhRvD, 72, 102002, doi: 10.1103/PhysRevD.72.102002

Eggleton, P. P. 1983, ApJ, 268, 368, doi: 10.1086/160960

Fehrmann, H., & Pletsch, H. J. 2014, PhRvD, 90, 124049, doi: 10.1103/PhysRevD.90.124049

Feroz, F., Hobson, M. P., Cameron, E., & Pettitt, A. N. 2013, ArXiv e-prints. https://arxiv.org/abs/1306.2144

Gaia Collaboration, Brown, A. G. A., Vallenari, A., et al. 2018, A&A, 616, A1, doi: 10.1051/0004-6361/201833051

Green, G. M., Schlafly, E., Zucker, C., Speagle, J. S., & Finkbeiner, D. 2019, ApJ, 887, 93, doi: 10.3847/1538-4357/ab5362

Hartman, R. C., Bertsch, D. L., Bloom, S. D., et al. 1999, ApJS, 123, 79, doi: 10.1086/313231

Hessels, J. W. T., Ransom, S. M., Stairs, I. H., et al. 2006, Science, 311, 1901, doi: 10.1126/science.1123430

Hunter, J. D. 2007, Computing in Science and Engineering, 9, 90, doi: 10.1109/MCSE.2007.55

Jones, D. I. 2010, MNRAS, 402, 2503, doi: 10.1111/j.1365-2966.2009.16059.x

—. 2015, MNRAS, 453, 53, doi: 10.1093/mnras/stv1584

Kandel, D., & Romani, R. W. 2020, ApJ, 892, 101, doi: 10.3847/1538-4357/ab7b62

Kaplan, D. L., Stovall, K., van Kerkwijk, M. H., Fremling, C., & Istrate, A. G. 2018, ApJ, 864, 15, doi: 10.3847/1538-4357/aad54c

Kerr, M. 2011, ApJ, 732, 38, doi: 10.1088/0004-637X/732/1/38

Kerr, M., Ray, P. S., Johnston, S., Shannon, R. M., & Camilo, F. 2015, ApJ, 814, 128, doi: 10.1088/0004-637X/814/2/128

Kong, A. K. H., Jin, R., Yen, T. C., et al. 2014, ApJL, 794, L22, doi: 10.1088/2041-8205/794/2/L22

Li, D., Wang, P., Qian, L., et al. 2018, IEEE Microwave Magazine, 19, 112, doi: 10.1109/MMM.2018.2802178

Lightkurve Collaboration, Cardoso, J. V. d. M. a., Hedges, C., et al. 2018, Lightkurve: Kepler and TESS time series analysis in Python. http://ascl.net/1812.013

LIGO Scientific Collaboration. 2018, LIGO Algorithm Library - LALSuite, free software (GPL), doi: 10.7935/GT1W-FZ16

Manchester, R. N., Hobbs, G. B., Teoh, A., & Hobbs, M. 2005, AJ, 129, 1993, doi: 10.1086/428488

McMillan, P. J. 2017, MNRAS, 465, 76, doi: 10.1093/mnras/stw2759

Nieder, L., Allen, B., Clark, C. J., & Pletsch, H. J. 2020, arXiv e-prints, arXiv:2004.11740. https://arxiv.org/abs/2004.11740

Nieder, L., Clark, C. J., Bassa, C. G., et al. 2019, ApJ, 883, 42, doi: 10.3847/1538-4357/ab357e

Oliphant, T. E. 2006, A guide to NumPy, Vol. 1 (Trelgol Publishing USA)

Pitkin, M. 2018, The Journal of Open Source Software, 3, 538, doi: 10.21105/joss.00538

Pitkin, M., Gill, C., Jones, D. I., Woan, G., & Davies, G. S. 2015, MNRAS, 453, 4399, doi: 10.1093/mnras/stv1931

Pitkin, M., Isi, M., Veitch, J., & Woan, G. 2017, arXiv e-prints, arXiv:1705.08978. https://arxiv.org/abs/1705.08978

Pletsch, H. J., & Clark, C. J. 2014, ApJ, 795, 75, doi: 10.1088/0004-637X/795/1/75

Pletsch, H. J., Guillemot, L., Fehrmann, H., et al. 2012, Science, 338, 1314, doi: 10.1126/science.1229054

Ransom, S. M., Eikenberry, S. S., & Middleditch, J. 2002, AJ, 124, 1788, doi: 10.1086/342285

Ransom, S. M., Ray, P. S., Camilo, F., et al. 2011, ApJL, 727, L16, doi: 10.1088/2041-8205/727/1/L16

Ray, P. S., Kerr, M., Parent, D., et al. 2011, ApJS, 194, 17, doi: 10.1088/0067-0049/194/2/17

Roberts, M. S. E. 2013, in IAU Symposium, Vol. 291, Neutron Stars and Pulsars: Challenges and Opportunities after 80 years, ed. J. van Leeuwen, 127–132, doi: 10.1017/S174392131202337X

Romani, R. W., Filippenko, A. V., & Cenko, S. B. 2014, ApJL, 793, L20, doi: 10.1088/2041-8205/793/1/L20

Sanchez, N., & Romani, R. W. 2017, ApJ, 845, 42, doi: 10.3847/1538-4357/aa7a02

Sanpa-arsa, S. 2016, PhD thesis, Graduate School of Arts and Sciences, University of Virginia, doi: 10.18130/V36K7P

Saz Parkinson, P. M., Xu, H., Yu, P. L. H., et al. 2016, ApJ, 820, 8, doi: 10.3847/0004-637X/820/1/8

Sengar, R., Tauris, T. M., Langer, N., & Istrate, A. G. 2017, MNRAS, 470, L6, doi: 10.1093/mnrasl/slx064

Shklovskii, I. S. 1970, Soviet Ast., 13, 562

Strader, J., Swihart, S., Chomiuk, L., et al. 2019, ApJ, 872, 42, doi: 10.3847/1538-4357/aafbaa

The LIGO Scientific Collaboration, the Virgo Collaboration, Abbott, R., et al. 2019, arXiv e-prints, arXiv:1912.11716. https://arxiv.org/abs/1912.11716

van der Walt, S., Colbert, S. C., & Varoquaux, G. 2011, Computing in Science and Engineering, 13, 22, doi: 10.1109/MCSE.2011.37

van Haarlem, M. P., Wise, M. W., Gunst, A. W., et al. 2013, A&A, 556, A2, doi: 10.1051/0004-6361/201220873

VanderPlas, J. T., & Ivezić, Ž. 2015, ApJ, 812, 18,
    doi: 10.1088/0004-637X/812/1/18